HHS Public Access

Author manuscript

Small. Author manuscript; available in PMC 2018 July 19.

Published in final edited form as:

Small. 2018 April ; 14(14): e1704181. doi:10.1002/smll.201704181.

Bioresponsive Microneedles with a Sheath Structure for H_2O_2 and pH Cascade-Triggered Insulin Delivery

Yuqi Zhang,
Joint Department of Biomedical Engineering, University of North Carolina at Chapel Hill and North Carolina State University, Raleigh, NC 27695, USA. Division of Molecular Pharmaceutics and Center for Nanotechnology in Drug Delivery, Eshelman School of Pharmacy, University of North Carolina at Chapel Hill, Chapel Hill, NC 27599, USA

Dr. Jinqiang Wang,
Joint Department of Biomedical Engineering, University of North Carolina at Chapel Hill and North Carolina State University, Raleigh, NC 27695, USA. Division of Molecular Pharmaceutics and Center for Nanotechnology in Drug Delivery, Eshelman School of Pharmacy, University of North Carolina at Chapel Hill, Chapel Hill, NC 27599, USA

Jicheng Yu,
Joint Department of Biomedical Engineering, University of North Carolina at Chapel Hill and North Carolina State University, Raleigh, NC 27695, USA. Division of Molecular Pharmaceutics and Center for Nanotechnology in Drug Delivery, Eshelman School of Pharmacy, University of North Carolina at Chapel Hill, Chapel Hill, NC 27599, USA

Dr. Di Wen,
Joint Department of Biomedical Engineering, University of North Carolina at Chapel Hill and North Carolina State University, Raleigh, NC 27695, USA. Division of Molecular Pharmaceutics and Center for Nanotechnology in Drug Delivery, Eshelman School of Pharmacy, University of North Carolina at Chapel Hill, Chapel Hill, NC 27599, USA

Anna R. Kahkoska,
Department of Medicine, University of North Carolina School of Medicine, Chapel Hill, NC 27599, USA

Dr. Yue Lu,
Joint Department of Biomedical Engineering, University of North Carolina at Chapel Hill and North Carolina State University, Raleigh, NC 27695, USA. Division of Molecular Pharmaceutics and Center for Nanotechnology in Drug Delivery, Eshelman School of Pharmacy, University of North Carolina at Chapel Hill, Chapel Hill, NC 27599, USA

Dr. Xudong Zhang,

Correspondence to: Jinqiang Wang; Zhen Gu.

Conflict of Interest
The authors declare no conflict of interest.

Supporting Information
Supporting Information is available from the Wiley Online Library or from the author.

Joint Department of Biomedical Engineering, University of North Carolina at Chapel Hill and North Carolina State University, Raleigh, NC 27695, USA. Division of Molecular Pharmaceutics and Center for Nanotechnology in Drug Delivery, Eshelman School of Pharmacy, University of North Carolina at Chapel Hill, Chapel Hill, NC 27599, USA

Prof. John B. Buse, and
Department of Medicine, University of North Carolina School of Medicine, Chapel Hill, NC 27599, USA

Prof. Zhen Gu
Joint Department of Biomedical Engineering, University of North Carolina at Chapel Hill and North Carolina State University, Raleigh, NC 27695, USA. Division of Molecular Pharmaceutics and Center for Nanotechnology in Drug Delivery, Eshelman School of Pharmacy, University of North Carolina at Chapel Hill, Chapel Hill, NC 27599, USA. Department of Medicine, University of North Carolina School of Medicine, Chapel Hill, NC 27599, USA

Abstract

Self-regulating glucose-responsive insulin delivery systems have great potential to improve clinical outcomes and quality of life among patients with diabetes. Herein, an H_2O_2-labile and positively charged amphiphilic diblock copolymer is synthesized, which is subsequently used to form nano-sized complex micelles (NCs) with insulin and glucose oxidase of pH-tunable negative charges. Both NCs are loaded into the crosslinked core of a microneedle array patch for transcutaneous delivery. The microneedle core is additionally coated with a thin sheath structure embedding H_2O_2-scavenging enzyme to mitigate the injury of H_2O_2 toward normal tissues. The resulting microneedle patch can release insulin with rapid responsiveness under hyperglycemic conditions owing to an oxidative and acidic environment because of glucose oxidation, and can therefore effectively regulate blood glucose levels within a normal range on a chemically induced type 1 diabetic mouse model with enhanced biocompatibility.

Keywords

diabetes; drug delivery; insulin; microneedles; stimuli-responsive

Diabetes mellitus is a global burden affecting 422 million people in 2016.[1] It is characterized by a deficit of endogenously produced insulin and thereafter elevated blood glucose levels (BGLs).[2] Open-loop subcutaneous injection of insulin cannot regulate BGLs tightly and is associated with a risk of severe hypoglycemia.[3] Thus, a closed-loop system that can “secret” desirable amounts of insulin in response to hyperglycemia while maintaining basal insulin release kinetics under normo-glycemia is urgently needed. Electronic closed-loop devices that have been developed to this end remain challenges associated with algorithm accuracy and sensor reliability.[4] Alternatively, chemically engineered formulations or devices with the assistance of glucose oxidase (GOx),[5] phenylboronic acid (PBA),[6] and glucose binding protein[7] have attracted increasing attention.[8] For example, GOx catalyzes the oxidation of glucose to gluconic acid in the presence of oxygen and generates hydrogen peroxide (H_2O_2).[9] Accordingly, GOx-mediated enzymatic reaction can create a local oxidative and acidic environment triggered

by elevated glucose levels to promote the release of insulin preloaded in acid-responsive systems.[10] However, the typical pH change-triggered response of materials is often accompanied by slow changes in the conformation and morphology of materials and formulations under a physiological condition.[5e] In addition, the in vivo release of GOx from medical devices may cause potential toxicity,[11] as well as the concerns over long-term biocompatibility of the H_2O_2 generated during oxidation of glucose.[12] Therefore, the ongoing development of smart insulin delivery systems is focused on achieving several merits, including rapid responsiveness, ease of preparation and administration, as well as excellent biocompatibility.[13]

Here, we describe a new glucose-responsive microneedle (MN) array patch[14] for self-regulated insulin delivery, utilizing H_2O_2 and pH cascade-responsive NCs. Briefly, insulin was first entrapped into degradable complex micelles (designated Ins-NCs); while GOx was encapsulated into non-degradable complex micelles (designated GOx-NCs) via crosslinking with uncleavable bonds (Scheme 1a). Both Ins-NCs and GOx-NCs were then loaded into the crosslinked gel core matrix of microneedle. Under a hyperglycemic condition, the Ins-NCs could respond to H_2O_2 and gluconic acid generated by the GOx-catalyzed oxidation of glucose and be dissociated to promote insulin release because of the disruption of micelle structure as well as charge reductions of polymer (positive charge) and insulin (negative charge) (Scheme 1a,b). Inspired by the protection function against oxidation in the peroxisome,[15] catalase nanogel (CAT-NG)[5b,c] was embedded into the crosslinked-poly(vinyl alcohol) (PVA) sheath structure, covering the surface of the microneedle core matrix (Scheme 1c), to mitigate the injury of H_2O_2 generated in the core part toward normal tissues (Scheme S1, Supporting Information). After painless administration of MN patch, Ins-NCs could be decomposed when MN was exposed to elevated interstitial fluid glucose under a hyperglycemic state, thereby rapidly releasing insulin to capillary vessels and consequently restoring homeostasis.

Through the atom transfer radical polymerization (ATRP) initiated by polyethylene glycolyl monomethyl ether 2-bromoisobutyrate ($MPEG_{5K}$-Br), 2-(dimethylamino)ethyl methacrylate (DMAEMA) was polymerized to obtain $MPEG_{5K}$-$P(DMAEMA)_{6K}$ (Figures S1 and S2a,b, Supporting Information), which was subsequently modified with 4-(bromomethyl)phenylboronic acid to obtain the positively charged $MPEG_{5K}$-P(DMAEMA-PBA)$_{14K}$ (Figure S3a,b, Supporting Information). In the presence of H_2O_2, phenylboronic acid on $MPEG_{5K}$-P(DMAEMA-PBA)$_{14K}$ was oxidized and hydrolyzed, generating $MPEG_{5K}$-$P(DMAEMA)_{6K}$ with reduced positive charge (Scheme 1b), as demonstrated by 1H-NMR (Figure S3a, Supporting Information).[16] In addition, poly(DMAEMA) and poly(DMAEMA-PBA) were synthesized via ATRP initiated by ethyl α-bromoisobutyrate and subsequent quaternarization by 4-(bromomethyl)phenylboronic acid, respectively (Figures S4a,b and S5a,b, Supporting Information). Given its isoelectric point of ≈5.3,[17] insulin is negatively charged at pH 7.4 and capable of complexing with positively charged $MPEG_{5K}$-P(DMAEMA-PBA)$_{14K}$[18] to form Ins-NCs with a PEG corona and a complex core.[19] To further stabilize the micelle structure, PVA was incorporated via forming acid-inert ester bonds between the phenylboronic acids on poly(DMAEMA-PBA) and *cis*-1, 3-diols on PVA.[20] Therefore, Ins-NCs with a loading capacity of 50 wt%, an average hydrodynamic size around 60 nm, and ζ-potential of 4.4 ± 0.5 mV were achieved as

measured by dynamic light scattering (DLS) (Figure 1a) and transmission electronic microscopy (TEM) (Figure 1b).[21] When Ins-NCs were degraded, the solution gradually became transparent after incubation with glucose (400 mg dL^{-1}) in the presence of GOx (Figure S6, Supporting Information). Meanwhile, GOx was also integrated into *m*-PVA stabilized nanocomplex micelles (GOx-NCs) with an average hydrodynamic size of around 50 nm (Figure S7, Supporting Information) and ζ-potential of 2.1 ± 0.4 mV. In addition, an undegradable network of *m*-PVA on GOx-NCs formed upon exposure to UV light (365 nm, 6 × 10 s). GOx-NCs had a GOx loading capacity of 33 wt%, and showed similar activity to native GOx regarding catalyzing the oxidation of glucose to produce H_2O_2 (Figure 1c).[22] Furthermore, a different pH value after GOx-NC catalysis indicated a glucose concentration-dependent manner of gluconic acid generation (Figure 1d). Next, the insulin release rate was evaluated in the presence of GOx in phosphate buffered saline (PBS) at pH 7.4 with three different glucose concentrations, including a typical hyperglycemic level (400 mg dL^{-1}), a normo-glycemic level (100 mg dL^{-1}), and a control level (0 mg dL^{-1}). The insulin release rate was remarkably promoted under a hyperglycemic state compared to those of other two groups (Figure 2a).

Furthermore, the mechanism of glucose-triggered insulin release was investigated. Prior to PVA crosslinking, instant insulin release was triggered in both 100 and 400 mg dL^{-1} glucose solution (Figure S8, Supporting Information). However, the addition of PVA stabilized the complex and significantly reduced insulin release in 100 mg dL^{-1} glucose solution (Figure 2a). Further studies indicated that neither H_2O_2 nor slightly acidic environment could individually achieve insulin release (Figure 2b). Moreover, insulin was found to be instantly released in slightly acidic pH from the complex that was pretreated with H_2O_2, indicating that the insulin was released in a cascade: (1) poly(DMAEMA-PBA) was oxidized and hydrolyzed to poly(DMAEMA), leading to reduced positive charge of polymer and crosslinking density of Ins-NCs; (2) the gradually decreased pH led to reduced negative charge or even charge reversal of insulin (from negative to positive charge under pH lower than isoelectronic point), thereby resulting in the dissociation of complex and subsequent release of insulin. This two-step pattern of insulin release endows the insulin delivery system enhanced safety for in vivo application to avoid the unwanted insulin release solely triggered by either H_2O_2 or acid, for example, generated in a nonrelevant condition of inflammation.[23] Moreover, the release rate of insulin from complex was steadily enhanced when gradually increasing the glucose concentrations of the tested solutions from normoglycemic to hyperglycemic conditions, where a 50-fold difference in insulin release rate was achieved in 1 h when the glucose concentration was increased from 100 to 400 mg dL^{-1} (Figure S9, Supporting Information). Additionally, the pulsatile release profile of insulin was achieved when the complex was alternatively exposed to the normoglycemic and hyperglycemic levels (Figure S10, Supporting Information).

The insulin and GOx release profiles from nanocomplex micelles encapsulated in *m*-PVA gel were critical for their in vivo application. The *m*-PVA gel was prepared from *m*-PVA aqueous solution via exposure to UV light in the presence of a radical initiator (Figure S11, Supporting Information). The release rate of insulin from Ins-NCs entrapped in the gel was twofold faster at a glucose concentration of 400 mg dL^{-1} than that of 100 mg dL^{-1} (Figure 2c). Meanwhile, the release rate of GOx was independent on glucose level and occurred in

negligible amounts due to the crosslinking of GOx-NCs by *m*-PVA (Figure 2d). Additionally, the far-UV circular dichroism spectra of the native and released insulin from gels were nearly identical, suggesting that the released insulin retained *α*-helical secondary structure associated with bioactivity (Figure S12, Supporting Information).

To facilitate the administration, Ins-NCs and GOx-NCs were integrated into an MN array patch. The MN array patch was prepared using a micromolding approach. First, the CAT was encapsulated into a CAT-NG (Figure S13, Supporting Information) to inhibit passive release of CAT.[5b] CAT-NG retained the activity of catalyzing H_2O_2 to H_2O (Figure S14, Supporting Information), and was then dissolved in an aqueous solution containing *m*-PVA and photoinitiator, loaded into a silicone micromold, and kept under reduced pressure for 30 min. After centrifugation, it was exposed to UV light (6 × 10 s) to crosslink the matrix to form an MN "sheath." Ins-NCs, GOx-NCs, and radical initiator dissolved in an aqueous solution containing PVA/*m*-PVA and polyvinylpyrrolidone (PVP) were then deposited in silicone molds to form an MN "core". The addition of a proper ratio of PVP has been shown to enhance the strength of microneedle for better skin penetration.[24] The resulting device was arranged in a 20 × 20 MN array on a patch. The needle had a conical shape (Figure 3a,b) and enough strength (Figure S15, Supporting Information).[25] In addition, fluorescein isothiocyanate (FITC)-labeled CAT-NG formed a sheath covering the PVA/*m*-PVA/PVP core loaded with the rhodamine B-labeled insulin as validated using fluorescence microscope (Figure 3c).

The in vivo performance of the MN array patches was evaluated utilizing a mouse model of type 1 diabetes induced by streptozotocin. The mice were divided into four groups treated with (1) CAT-NG-coated MN array patch loaded with GOx-NCs and Ins-NCs (MN-(G+C+I)); (2) subcutaneous injection of human recombinant insulin; (3) microneedle array patch loaded with blank PVA/*m*-PVA and PVP (MN-Gel); and (4) CAT-NG-coated MN array patch of Ins-NCs (MN-(C+I)). The staining by trypan blue indicated successful penetration of MNs into the excised skin (Figure S16, Supporting Information). Besides, the temporal microchannels on the skin caused by MNs could quickly recover within 2 h post-treatment (Figure S17, Supporting Information).

BGLs of the mice were monitored over time following treatment with MN patches. It was observed that the BGLs of mice treated by MN-(G+C+I) were quickly decreased to around 100 mg dL^{-1} in 30 min post-administration and maintained below 200 mg dL^{-1} for almost 4 h, considerably longer than those of the mice subcutaneously injected with insulin (Figure 4a). This fast dynamic in BGL change was attributed to the rapid establishment of the local oxidative and acidic environment through oxidation of glucose absorbed from interstitial fluid, which has a similar glucose level to that in blood,[26] as well as the high sensitivity of Ins-NCs to these stimuli. In contrast, the negligible BGL reduction was observed in the mice treated with MN-(C+I) and MN-Gel. Additionally, the plasma human insulin levels in mice treated with MN-(G+C+I) were significantly higher than those treated with MN-(C+I) (Figure 4b).

Moreover, the intraperitoneal glucose tolerance test was carried out 1 h post-administration of MNs or insulin. A spike in BGLs was observed for all groups after the intraperitoneal

injection of glucose. However, only healthy mice and MN-(G+C+I) could restore blood glucose levels to a normoglycemic level within a short period, and the mice treated with MN-(G+C+I) showed significantly enhanced glucose tolerance to the glucose challenge (Figure S18, Supporting Information). To assess the risk of hypoglycemia associated with treatment by MN-(G+C+I), the BGLs of healthy mice treated with different MN array patches were observed. The BGLs of mice treated with insulin showed a remarkable decrease, while the BGLs of mice treated with MN-(G+C+I) showed only a slight decrease, consistent with the slow release of insulin from gels under a normoglycemic state (Figure S19a, Supporting Information). Additionally, the MN-(G+C+I)-treated group showed significantly lower hypoglycemia index than insulin (Figure S19b, Supporting Information).

Importantly, the matrix materials used for insulin delivery have shown negligible in vitro cytotoxicity (Figure S20, Supporting Information). For in vivo toxicity, compared to the skin tissues treated by MN-Gel (Figure 4c), a clear damage of skin tissue was observed for MN-(G+I). In sharp contrast, only negligible inflammation was observed on the skin of mice treated with MN-(G+C+I) due to the presence of a CAT-embedded sheath (Figure 4c). These findings were further validated by hematoxylin and eosin (H&E) staining results. Compared with the skin treated with MN-Gel (Figure S21, Supporting Information), the skin samples treated with MN-(G+I) (Figure S21, Supporting Information) were significantly thicker and showed apparent neutrophil infiltration, indicating a pathophysiological response and tissue damage induced by H_2O_2.[27] However, reduced neutrophil infiltration was observed in skin samples from mice treated with MN-(G+C+I) (Figure 4d). Additionally, the skin tissue stained with the in situ terminal deoxynucleotidyl transferase deoxyuridine triphosphate (dUTP) nick end labeling (TUNEL) assay clearly demonstrated the negligible cell apoptosis in the skin sample treated with MN-(G+C+I) as compared to that associated with the control group (Figure 4d and Figure S21, Supporting Information). Accordingly, the counts of white blood cells from mice treated by MN-(G+C+I) were similar to that of the healthy mice (Figure 4e). For the long-term usage, the frequent exposure of skin tissues to the leaking H_2O_2 could cause some side effects. However, with the optimization of the ratio of CAT and GOx, as well as regular change of the MN administration position, the side effects toward skin could be minimized for daily usage. The animal study protocol was approved by the Institutional Animal Care and Use Committee at North Carolina State University and the University of North Carolina at Chapel Hill.

In summary, we have developed a new MN-array patch with a sheath structure, loaded with dual sequential stimuli-responsive nanocomplex micelles for self-regulated insulin delivery. It was demonstrated that this patch could rapidly and safely release insulin triggered by locally generated H_2O_2 and an acidic microenvironment under a hyperglycemic condition. In vivo experiments indicated that the MN-(G+C+I) was effective in regulating BGLs under a normoglycemic state while reducing the risk of hypoglycemia. Importantly, utilization of CAT sheath-like coating significantly mitigated the skin inflammation caused by the production of H_2O_2.

Supplementary Material

Refer to Web version on PubMed Central for supplementary material.

Acknowledgments

Y.Z. and J.W. contributed equally to this work. This work was supported by the startup grant from the North Carolina State University and University of North Carolina at Chapel Hill, National Science Foundation (Grant No. 1708620), and JDRF (Grant No. 2-SRA- 2016-269- A-N) to Z.G. This work was performed in part at the Analytical Instrumentation Facility (AIF) at North Carolina State University, which is supported by the State of North Carolina and the National Science Foundation (Grant No. 1542015). The AIF is a member of the North Carolina Research Triangle Nanotechnology Network (RTNN), a site in the National Nanotechnology Coordinated Infrastructure (NNCI).

References

1. Mo R, Jiang T, Di J, Tai W, Gu Z. Chem Soc Rev. 2014; 43:3595. [PubMed: 24626293]
2. a) Mo R, Jiang T, Di J, Tai W, Gu Z. Chem Soc Rev. 2014; 43:3595. [PubMed: 24626293] b) Veiseh O, Tang BC, Whitehead KA, Anderson DG, Langer R. Nat Rev Drug Discovery. 2015; 14:45. [PubMed: 25430866]
3. a) Ohkubo Y, Kishikawa H, Araki E, Miyata T, Isami S, Motoyoshi S, Kojima Y, Furuyoshi N, Shichiri M. Diabetes Res Clin Pract. 1995; 28:103. [PubMed: 7587918] b) Owens DR, Zinman B, Bolli GB. Lancet. 2001; 358:739. [PubMed: 11551598]
4. a) Cengiz E, Sherr JL, Weinzimer SA, Tamborlane WV. Expert Rev Med Devices. 2011; 8:449. [PubMed: 21728731] b) Bequette B. Diabetes Technol Ther. 2005; 7:28. [PubMed: 15738702]
5. a) Peppas NA, Huang Y, Torres-Lugo M, Ward JH, Zhang J. Annu Rev Biomed Eng. 2000; 2:9. [PubMed: 11701505] b) Gu Z, Aimetti AA, Wang Q, Dang TT, Zhang Y, Veiseh O, Cheng H, Langer RS, Anderson DG. ACS Nano. 2013; 7:4194. [PubMed: 23638642] c) Gu Z, Dang TT, Ma M, Tang BC, Cheng H, Jiang S, Dong Y, Zhang Y, Anderson DG. ACS Nano. 2013; 7:6758. [PubMed: 23834678] d) Yu J, Zhang Y, Ye Y, DiSanto R, Sun W, Ranson D, Ligler FS, Buse JB, Gu Z. Proc Natl Acad Sci USA. 2015; 112:8260. [PubMed: 26100900] e) Tai W, Mo R, Di J, Subramanian V, Gu X, Buse JB, Gu Z. Biomacromolecules. 2014; 15:3495. [PubMed: 25268758] f) Podual K, Doyle FJ, Peppas NA. J Controlled Release. 2000; 67:9.g) Podual K. Polymer. 2000; 41:3975.h) Zhang K, Wu XY. J Controlled Release. 2002; 80:169.
6. a) Brooks WLA, Sumerlin BS. Chem Rev. 2016; 116:1375. [PubMed: 26367140] b) Chou DHC, Webber MJ, Tang BC, Lin AB, Thapa LS, Deng D, Truong JV, Cortinas AB, Langer R, Anderson DG. Proc Natl Acad Sci USA. 2015; 112:2401. [PubMed: 25675515] c) Kataoka K, Miyazaki H, Bunya M, Okano T, Sakurai Y. J Am Chem Soc. 1998; 120:12694.d) Matsumoto A, Yoshida R, Kataoka K. Biomacromolecules. 2004; 5:1038. [PubMed: 15132698] e) Dong Y, Wang W, Veiseh O, Appel EA, Xue K, Webber MJ, Tang BC, Yang XW, Weir GC, Langer R, Anderson DG. Langmuir. 2016; 32:8743. [PubMed: 27455412] f) Matsumoto A, Kurata T, Shiino D, Kataoka K. Macromolecules. 2004; 37:1502.g) Shiino D, Murata Y, Kubo A, Kim YJ, Kataoka K, Koyama Y, Kikuchi A, Yokoyama M, Sakurai Y, Okano T. J Controlled Release. 1995; 37:269.
7. a) Obaidat AA, Park K. Pharm Res. 1996; 13:989. [PubMed: 8842034] b) Brownlee M, Cerami A. Diabetes. 1983; 32:499. [PubMed: 6354778] c) Brownlee M, Cerami A. Science. 1979; 206:1190. [PubMed: 505005] d) Liu F, Song SC, Mix D, Baudy M, Kim SW. Bioconjugate Chem. 1997; 8:664.e) Joel S, Turner KB, Daunert S. ACS Chem Biol. 2014; 9:1595. [PubMed: 24841549] f) Wang C, Ye YQ, Sun WJ, Yu JC, Wang JQ, Lawrence DS, Buse JB, Gu Z. Adv Mater. 2017; 29:1606617.
8. a) Gordijo CR, Koulajian K, Shuhendler AJ, Bonifacio LD, Huang HY, Chiang S, Ozin GA, Giacca A, Wu XY. Adv Funct Mater. 2011; 21:73.b) Bratlie KM, York RL, Invernale MA, Langer R, Anderson DG. Adv Healthcare Mater. 2012; 1:267.c) Hassan CM, Doyle FJ, Peppas NA. Macromolecules. 1997; 30:6166.d) Yu J, Zhang Y, Bomba H, Gu Z. Bioeng Transl Med. 2016; 1:323. [PubMed: 29147685] e) Bakh NA, Cortinas AB, Weiss MA, Langer RS, Anderson DG, Gu Z, Dutta S, Strano MS. Nat Chem. 2017; 9:937. [PubMed: 28937662]
9. Wong CM, Wong KH, Chen XD. Appl Microbiol Biotechnol. 2008; 78:927. [PubMed: 18330562]
10. a) Yu J, Qian C, Zhang Y, Cui Z, Zhu Y, Shen Q, Ligler FS, Buse JB, Gu Z. Nano Lett. 2017; 17:733. [PubMed: 28079384] b) Hu X, Yu J, Qian C, Lu Y, Kahkoska AR, Xie Z, Jing X, Buse JB, Gu Z. ACS Nano. 2017; 11:613. [PubMed: 28051306]
11. Broom WA, Coulthard CE, Gurd MR, Sharpe ME. Br J Pharmacol Chemother. 1946; 1:225.

12. Saravanakumar G, Kim J, Kim WJ. Adv Sci. 2017; 4:1600124.
13. a) Sun W, Hu Q, Ji W, Wright G, Gu Z. Physiol Rev. 2017; 97:189.b) Peppas NA, Khademhosseini A. Nature. 2016; 540:335. [PubMed: 27974790] c) Lu Y, Aimetti AA, Langer R, Gu Z. Nat Rev Mater. 2017; 2:16075.
14. a) Yu J, Zhang Y, Kahkoska AR, Gu Z. Curr Opin Biotechnol. 2017; 48:28. [PubMed: 28292673] b) Prausnitz MR. Annu Rev Chem Biomol Eng. 2017; 8:177. [PubMed: 28375775]
15. De Duve C, Baudhuin P. Physiol Rev. 1966; 46:323. [PubMed: 5325972]
16. Liu X, Xiang J, Zhu D, Jiang L, Zhou Z, Tang J, Liu X, Huang Y, Shen Y. Adv Mater. 2016; 28:1743. [PubMed: 26663349]
17. Wintersteiner O, Abramson HA. J Biol Chem. 1933; 99:741.
18. Scott D, Fisher A. J Pharmacol Exp Ther. 1936; 58:78.
19. Park W, Kim D, Kang HC, Bae YH, Na K. Biomaterials. 2012; 33:8848. [PubMed: 22959184]
20. Piest M, Zhang X, Trinidad J, Engbersen JFJ. Soft Matter. 2011; 7:11111.
21. a) Piest M, Zhang X, Trinidad J, Engbersen JFJ. Soft Matter. 2011; 7:11111.b) Springsteen G, Wang B. Tetrahedron. 2002; 58:5291.
22. Yamamoto Y, Koma H, Yagami T. NeuroToxicology. 2015; 49:86. [PubMed: 26038286]
23. Balkwill F. Eur J Cancer. 2006; 42:689.
24. Lee I-C, He J-S, Tsai M-T, Lin K-C. J Mater Chem B. 2015; 3:276.
25. a) Olatunji O, Das DB, Garland MJ, Belaid L, Donnelly RF. J Pharm Sci. 2013; 102:1209. [PubMed: 23359221] b) Davis SP, Landis BJ, Adams ZH, Allen MG, Prausnitz MR. J Biomech. 2004; 37:1155. [PubMed: 15212920]
26. Thennadil SN, Rennert JL, Wenzel BJ, Hazen KH, Ruchti TL, Block MB. Diabetes Technol Ther. 2001; 3:357. [PubMed: 11762514]
27. Liu Y, Du J, Yan M, Lau MY, Hu J, Han H, Yang OO, Liang S, Wei W, Wang H, Li J, Zhu X, Shi L, Chen W, Ji C, Lu Y. Nat Nanotechnol. 2013; 8:187. [PubMed: 23416793]

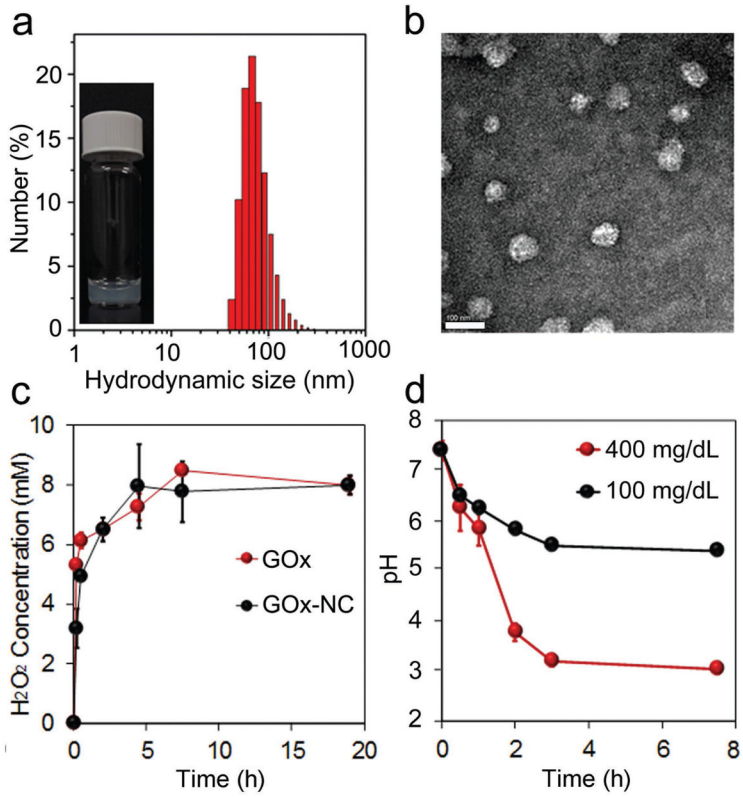

Figure 1.

Characterizations of Ins-NCs and GOx-NCs. a) Representative image of Ins-NC solution and hydrodynamic size distribution of Ins-NCs as determined by DLS. Inset: A representative picture of the Ins-NC solution sample (insulin concentration: 1 mg mL^{-1}). b) Representative TEM image of Ins-NCs. Scale bar, 100 nm. c) H_2O_2 generation in PBS (10×10^{-3} M, pH 7.4) containing glucose (400 mg dL^{-1}) as catalyzed by GOx and GOx-NCs. d) The pH change of PBS solution of various glucose concentrations (100 or 400 mg dL^{-1}) in the presence of GOx-NCs (0.2 mg mL^{-1} GOx-eq. concentration). Data points represent mean ± SD ($n = 3$). Error bars indicate SD.

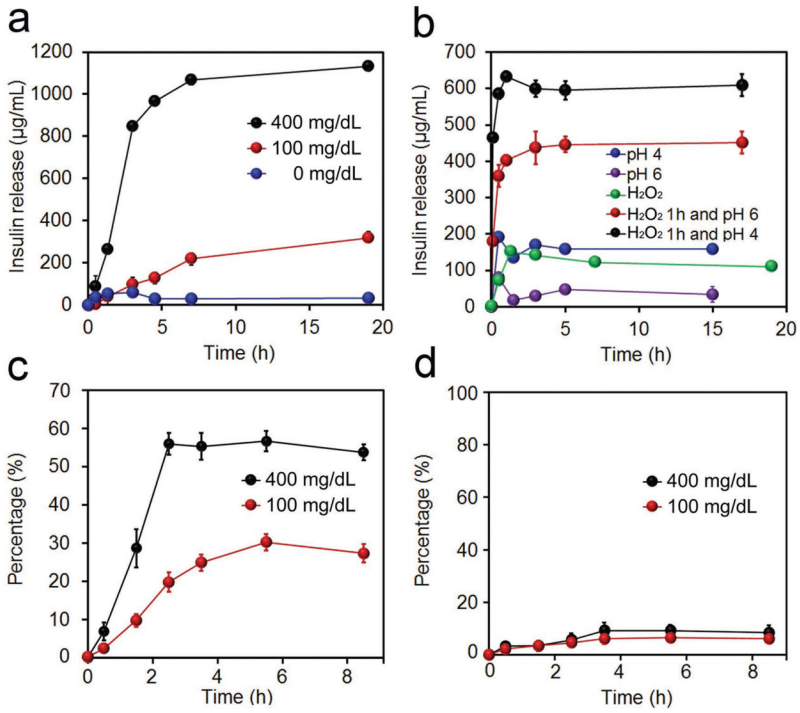

Figure 2.

In vitro characterization of glucose-responsive insulin release. a) Glucose concentration-dependent insulin release from a complex of insulin in PBS 7.4 in the presence of GOx (0.2 mg mL^{-1}). The glucose concentration was set as 0, 100, and 400 mg dL^{-1}. b) H_2O_2 (5×10^{-3} M) and pH cascade-triggered insulin release from a complex of insulin. c) Glucose concentration-dependent insulin release from Ins-NCs loaded in *m*-PVA gel in PBS 7.4 in the presence of GOx (0.2 mg mL^{-1}). d) Glucose concentration-dependent GOx release from GOx-NCs encapsulated in *m*-PVA gel in PBS 7.4. Additional GOx (0.2 mg mL^{-1}) was added. The glucose concentration was set as 100 and 400 mg dL^{-1}. Data points represent mean ± SD ($n = 3$). Error bars indicate SD.

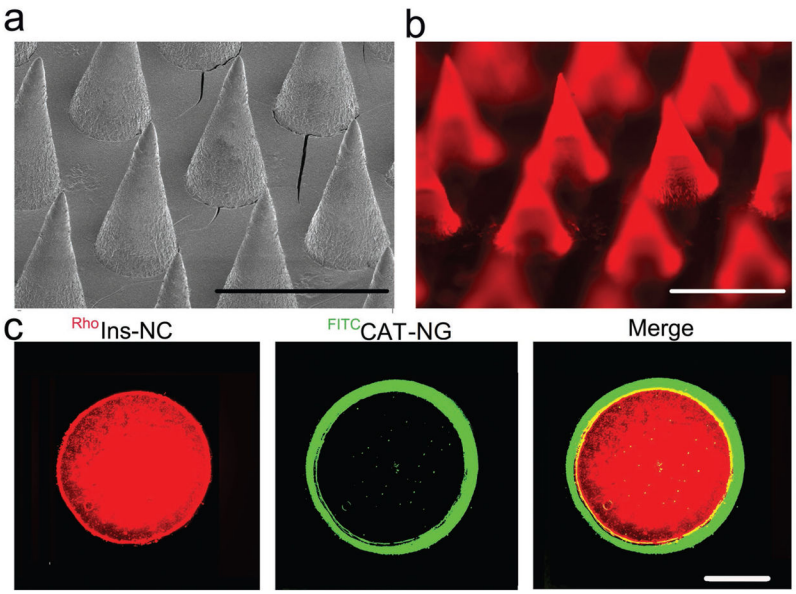

Figure 3.

Characterization of the MN array patch with a sheath structure. a) Representative scanning electron microscopy (SEM) image of microneedle array patch. Scale bar, 600 μm. b) Representative fluorescence microscopy image of MN arrays loaded with rhodamine B-labeled insulin. Scale bar, 600 μm. c) Representative images of a cross-section of MN with a CAT-NG sheath:rhodamine B-labeled insulin (red), FITC-labeled CAT sheath layer (green), and merging of both images. The sheath layer was 23 ± 6 μm thick as analyzed using software ImageJ. Scale bar, 100 μm.

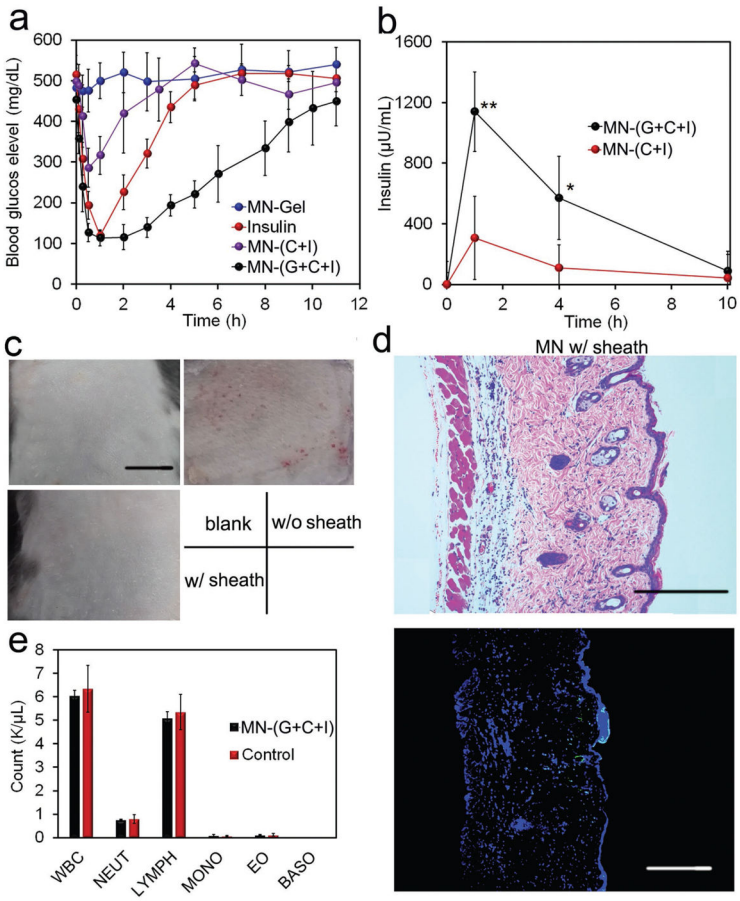

Figure 4.

In vivo evaluation of MN array patches for type 1 diabetes treatment. a) Blood glucose levels of type 1 diabetic mice treated with various kinds of microneedle array patches. b) Blood insulin level of mice treated with MN array patches. Data points represent mean ± SD (n = 3). *P < 0.05, **P < 0.01 (analyzed by two-tailed Student's t-test) for MN-(G+C+I) compared with control MN-(C+I). c) Representative images of skins at the treated site of mice. Mice were treated with MN-Gel, MN-(G+I), and MN-(G+C+I) for 12 h, and the skins were gathered after the mice were euthanized. Scale bars, 1 cm. d) H&E staining and immunohistologic staining with TUNEL assay (green) and Hoechst (blue) of skins treated with MN-(G+C+I). Scale bars, 300 μm. e) Analysis of blood white cells of mice treated with MN-(G+C+I). Blood samples were obtained 2 d post-treatment. WBC: white blood cells; NEUT: neutrophils; LYMPH: lymphocytes; MONO: monocytes; EO: eosinophils; BASO: basophils.

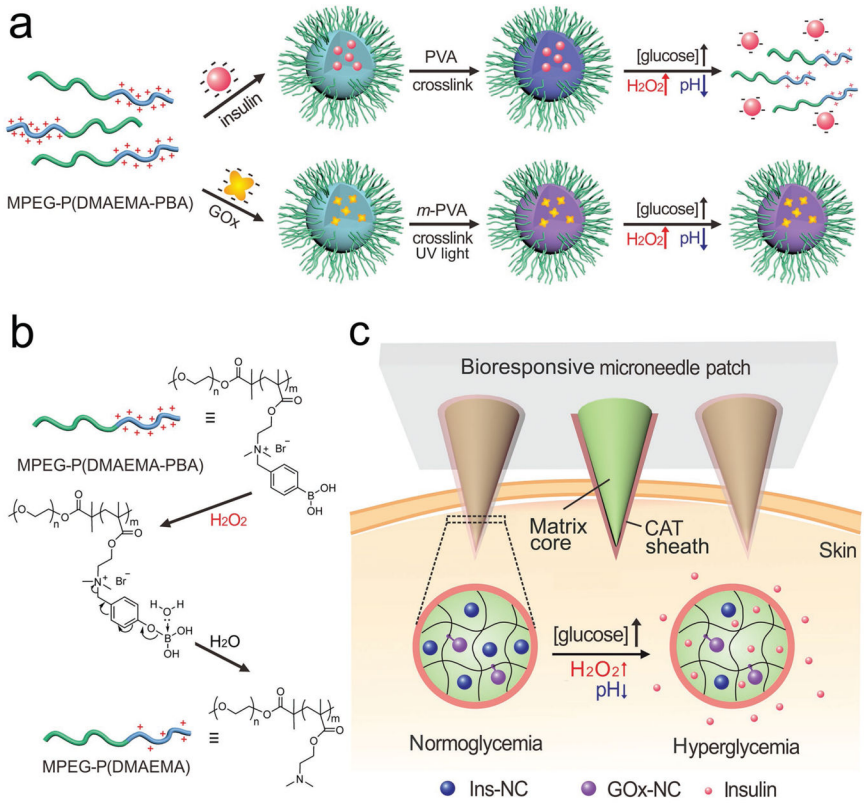

Scheme 1.

Schematic of the glucose-responsive insulin delivery system utilizing H_2O_2 and pH cascade-responsive NC-loading MN-array patch. a) Formation of Ins-NCs and GOx-NCs and mechanism of glucose-responsive insulin release. b) Schematic of H_2O_2-triggered charge reduction of the polymer. c) Schematic of the NC-containing MN-array patch with a CAT sheath structure for in vivo insulin delivery. Insulin release is triggered under a hyperglycemic state.